

Relation between Pore Sizes of Protein Crystals and Anisotropic Solute Diffusivities

Aleksandar Cvetkovic,[†] Cristian Picioareanu,[†] Adrie J. J. Straathof,^{*,†}
Rajamani Krishna,[‡] and Luuk A. M. van der Wielen[†]

Contribution from the Department of Biotechnology, Delft University of Technology,
Julianalaan 67, 2628 BC Delft, The Netherlands, Van't Hoff Institute for Molecular Sciences,
University of Amsterdam, Nieuwe Achtergracht 166, 1018 WV Amsterdam, The Netherlands

Received September 29, 2004; E-mail: A.J.J.Straathof@tnw.tudelft.nl

Abstract: The diffusion of a solute, fluorescein, into lysozyme protein crystals with different pore structures was investigated. To determine the diffusion coefficients, three-dimensional solute concentration fields acquired by confocal laser scanning microscopy (CLSM) during diffusion into the crystals were compared with the output of a time-dependent 3-D diffusion model. The diffusion process was found to be anisotropic, and the degree of anisotropy increased in the order: triclinic, tetragonal and orthorhombic crystal morphology. A linear correlation between the pore diffusion coefficients and the pore sizes was established. The maximum size of the solute, deduced from the established correlation of diffusion coefficients and pore size, was 0.73 ± 0.06 nm, which was in the range of the average diameter of fluorescein (0.69 ± 0.02 nm). This proves that size exclusion is the key mechanism for solute diffusion in protein crystals. Hence, the origin of solute diffusion anisotropy can be found in the packing of the protein molecules in the crystals, which determines the crystal pore organization.

Introduction

For practical applications, crystalline forms of enzymes and other proteins have substantial advantages over their amorphous and immobilized counterparts.^{1–3} They are the proteins in their most compact active form characterized by the highest volumetric activity.⁴ Chemical cross-linking of the protein crystals maintains the crystalline state of proteins outside the crystallization conditions and also reinforces the crystal structure,^{5–7} making their practical application possible.^{8,9} The wide variety of molecular topologies found in protein crystals classifies them as nanoporous materials that are biochemical cousins of zeolites and silica–alumina–phosphates at the unit cell level.⁸ Due to their characteristics, protein crystals have great potential in separation of enantiomers and other compounds, in medical formulations,¹ in detergents,¹ in biosensors¹⁰ and in biocatalysis.¹

However, the use of protein crystals is still not fully exploited. The full activity of an enzyme crystal cannot be achieved easily

because of mass-transfer limitations.^{11,12} For this purpose, much smaller and homogeneous crystals than those used in X-ray studies would be preferred to maximize the surface area-to-volume ratio while preserving crystal characteristics.¹³ Furthermore, improvement of crystallization by crystallizing other proteins or protein-like molecules, producing more uniform crystal with specific crystal size on the large (industrial) scale would give the impetus needed for their applications. Recent findings provided the precursors needed—protein nanocrystals have been produced and characterized,¹⁴ large scale crystallization processes for production of uniform protein crystals with sharp cutoff crystal sizes have been described and developed,¹⁵ and crystals made of monoclonal antibodies have successfully been developed and applied in the enantioselective separation of drug enantiomers.¹⁶

In contrast to the improvement of the protein crystal as a separation or catalytic material, understanding of the transport mechanism, which is essential in any successful implementation of crystalline proteins, is still insufficient and needs to be further investigated. Methods for experimental determination of the solute transport in protein crystals have been the subject of several studies.^{13,17–22} In most of these studies, overall effective diffusion coefficients were applied to describe solute

[†] Department of Biotechnology, Delft University of Technology.

[‡] Van't Hoff Institute for Molecular Sciences, University of Amsterdam.

- (1) Margolin, A. L.; Navia, M. A. *Angew. Chem. Int. Ed.* **2001**, *40*, 2205–2222.
- (2) Klivanov, A. M. *Nature* **2001**, *409*, 241–246.
- (3) Jen, A.; Merkle, H. P. *Pharmaceut. Res.* **2002**, *18*, 1483–1488.
- (4) St Clair, N. L.; Shenoy, B.; Jacob, L. D.; Margolin, A. L. *Proc. Nat. Acad. Sci.* **1999**, *96*, 9469–9474.
- (5) Brange, J.; Langkjaer, L.; Havelund, S.; Volund, A. *Pharmaceut. Res.* **1992**, *9*, 715–726.
- (6) St Clair, N. L.; Navia, M. A. *J. Am. Chem. Soc.* **1992**, *114*, 7314–7316.
- (7) Quijoch, F. A.; Richards, F. M. *Biochemistry* **1966**, *5*, 4062–4076.
- (8) Vilenchik, L. Z.; Griffith, J. P.; St Clair, N.; Navia, M. A.; Margolin, A. L. *J. Am. Chem. Soc.* **1998**, *120*, 4290–4294.
- (9) Pastinen, O.; Jokela, J.; Eerikainen, T.; Schwabe, T.; Leisola, M. *Enzyme Microb. Technol.* **2000**, *26*, 550–558.
- (10) Morozov, V. N.; Morozova, T. Y. *Anal. Biochem.* **1992**, *201*, 68–79.

- (11) Doscher, M. S.; Richards, F. M. *J. Biol. Chem.* **1963**, *238*, 2399–2406.
- (12) Genzel, L.; Keilmann, F.; Martin, T. P.; Winterling, G.; Yacoby, Y.; Fröhlich, H.; Makinen, M. W. *Biopolymers* **1976**, *15*, 219–225.
- (13) Bishop, W. H.; Richards, F. M. *J. Mol. Biol.* **1968**, *38*, 315–328.
- (14) Martin, R. W.; Zilm, K. W. *J. Magn. Reson.* **2003**, *165*, 162–174.
- (15) Vuolanto, A.; Uotila, S.; Leisola, M.; Visuri, K. *J. Cryst. Growth* **2003**, *257*, 403–411.
- (16) Vuolanto, A.; Kiviharju, K.; Nevanen, T. K.; Leisola, M.; Jokela, J. *Cryst. Growth Des.* **2003**, *3*, 777–782.

transport.^{13,17–22} However, attempts to explain experimentally obtained overall effective diffusivities on the basis of solute or solution characteristics,^{13,18,19,22} or crystal density or porosity¹⁸ were unsuccessful. This was due to the averaging character of overall effective diffusivity, which neglects any impact of the crystal pore structure on the diffusion process.¹⁸ Developments in microtome techniques^{17,20} and CLSM¹⁸ have enabled determination of the effective pore diffusivities and have demonstrated anisotropy of diffusion in protein crystals. Although these studies assume that anisotropy of diffusion originates from the anisotropy of pore organization, they did not provide quantitative support for this claim. In our previous work,¹⁸ diffusion profiles for initial diffusion times were used to determine diffusivities in the crystal pore, simplifying the 3-D diffusion problem into three 1-D diffusion problems. This resulted in the determination of the diffusivities from only one diffusion profile in every crystal direction, raising questions on precision and validity of the determined diffusivities, especially because of the anisotropy.

The aim of this study is to find the mechanism that determines the origin of the anisotropy of the diffusion of solutes in protein crystals. For this purpose, a more reliable diffusion model is needed. A dynamic three-dimensional model will be presented for simultaneous determination of fluorescein diffusivities in the three orthogonal directions of un-cross-linked lysozyme crystals, using the experimental data for fluorescein uptake from its mother liquor solution by orthorhombic, tetragonal and triclinic lysozyme crystal morphology previously determined.¹⁸ The resulting orthogonal diffusivities will be compared with the pore sizes to acquire understanding of the mechanism of diffusion.

Methods

Processing of CLSM Images. Images obtained by CLSM¹⁸ were processed using the DIPImage toolbox of Matlab (Natick, MA). A crystal was labeled and rotated to a position parallel to the image frames. For each optical slice, an additional binary image representing the crystal position in the original image was made by setting the pixels inside the crystal on 1 and outside the crystal on 0. The position of every voxel in the 3-D CLSM image was determined relative to the arbitrary point chosen to be in the upper right corner of the confocal image closest to the microscope objective. As a result of the data extraction, a matrix was created for every confocal 3-D image. The matrix (saved as a text file) consisted of pixel positions in the image (x , y , and z), pixel positions relative to the crystal (0 or 1) and the intensity value of the pixels. Such matrixes containing pixel information acquired at different times were the input of a computer program for 3-D modeling of the anisotropic diffusion in crystals.

The grid sizes in the lateral crystal directions, Δx and Δy , were directly taken from the confocal image as the pixel size. In the axial direction, the size of the grid Δz was equal to the step used in the optical cutting for systems with constant refractive index. Before the performing diffusion computations, a correction procedure was applied to the experimental data to correct for anomalies induced by refractive index mismatch, as described elsewhere.¹⁸

Modeling the Anisotropic Diffusion Coefficients. Diffusion Equation. The diffusion of fluorescein into lysozyme crystals occurs in two stages. First, the external diffusion transports the solute from the solution to the crystal surface. Then, fluorescein diffuses from the surface to the interior of the crystal. Fluorescein diffusivity in water is 3 to 5 orders of magnitude higher than in the crystals,¹⁸ therefore diffusion

inside the crystal is the rate-limiting step. We assume that internal diffusion occurs only in the nanopores, with an effective diffusion coefficient D_e , which represents the value in free solution reduced by the effects of finite interstitial volume, tortuosity and hindrance.²³ In general, this interstitial diffusion is coupled to fluorescein adsorption, resulting in the equation

$$\epsilon \cdot \frac{\partial C_p}{\partial t} + \frac{\partial q_t}{\partial t} = \nabla(D_e \nabla C_p) \quad (1)$$

where C_p is the local interstitial concentration of fluorescein (kg m^{-3} crystal pores), q_t is the concentration of adsorbed fluorescein (kg m^{-3} total crystal volume) and ϵ is the crystal porosity (m^3 pores m^{-3} crystal). Considering that there was no significant adsorption of fluorescein in the protein crystals at the experimentally used solute concentrations,²⁴ and that diffusivity was uniform in space ($\nabla D_e = 0$), we get a simplified diffusion equation

$$\frac{\partial C_p}{\partial t} = D_p \cdot \nabla^2 C_p \quad (2)$$

with a pore diffusion coefficient D_p ($\text{m}^2 \text{s}^{-1}$) as a parameter, defined by

$$D_p = \frac{D_e}{\epsilon + K} \quad (3)$$

K is the partitioning coefficient of fluorescein, with a value as shown in Table 1.

Diffusion inside the porous crystals depends largely on size and connectivity of the pores. For this reason, the anisotropic crystal pore structure will induce diffusion anisotropy, usually represented in the following diffusivity matrix²⁵

$$D = \begin{pmatrix} D_{xx} & D_{xy} & D_{xz} \\ D_{yx} & D_{yy} & D_{yz} \\ D_{zx} & D_{zy} & D_{zz} \end{pmatrix} \quad (4)$$

where D_{ii} is the pore diffusivity (D_p) in the orthogonal crystal directions (the diagonal elements of the diffusion matrix) and D_{ij} is the cross diffusivity between direction i and j ($i = x, y, \text{ or } z; j = x, y, \text{ or } z$ and $i \neq j$). Furthermore, $D_{ij} = D_{ji}$ was assumed to decrease the number of parameters to be fitted. Consequently, the subsequent time-dependent diffusion equation was used for modeling the experimental data²⁵

$$\frac{\partial C_p}{\partial t} = D_{xx} \frac{\partial^2 C_p}{\partial x^2} + D_{yy} \frac{\partial^2 C_p}{\partial y^2} + D_{zz} \frac{\partial^2 C_p}{\partial z^2} + 2D_{xy} \frac{\partial^2 C_p}{\partial x \partial y} + 2D_{zx} \frac{\partial^2 C_p}{\partial z \partial x} + 2D_{yz} \frac{\partial^2 C_p}{\partial y \partial z} \quad (5)$$

Diffusion Coefficients. Considering the fundamental interest in the understanding the diffusion mechanism in crystals, three sets of diffusion matrixes (called here sub-models) were applied to determine diffusivities by eq 5. The first sub-model was based on the assumption that diffusion in the crystal depends only on the diagonal and not on the cross-diffusivities (D_{ij} set to zero). The second and third sub-models take into account the complete diffusion matrix with the assumption

- (17) Botin, A. S.; Morozov, V. N. *Biofizika* **1985**, *32*, 22–28.
- (18) Cvetkovic, A.; Straathof, A. J. J.; Hanlon, D. N.; van der Zwaag, S.; Krishna, R.; van der Wielen, L. A. M. *Biotechnol. Bioeng.* **2004**, *86*, 389–398.
- (19) Granick, S. *J. Gen. Physiol.* **1942**, *25*, 571–578.
- (20) Morozov, V. N.; Kachalova, G. S.; Evtodienko, V. U.; Lanina, N. F.; Morozova, T. Y. *Eur. Biophys. J.* **1995**, *24*, 93–98.
- (21) O'Hara, P.; Goodwin, P.; Stoddard, B. L. *J. Appl. Cryst.* **1995**, *28*, 829–834.
- (22) Velev, O. D.; Kaler, E. W.; Lenhoff, A. M. *J. Phys. Chem. B* **2000**, *104*, 9267–9275.
- (23) Deen, W. M. *AIChE J.* **1987**, *33*, 1409–1425.
- (24) Cvetkovic, A.; Zomerdijk, M.; Straathof, A. J. J.; Krishna, R.; van der Wielen, L. A. M. *Biotechnol. Bioeng.* **2004**, *87*, 658–668.
- (25) Crank, J. *Mathematics of Diffusion*; Oxford Science Publications Clarendon Press: New York, 1995.

Table 1. Characteristics of the Lysozyme Crystal Structures and Diffusion Parameters (including 95% confidence interval) Estimated for Fluorescein Transport in Lysozyme Crystals Using Eq 5 and from Literature^{18a}

crystal structure	PDB name	ionic strength ^b mol.L ⁻¹	density ^b kg/m ³	pH	solvent content ^b (v/v)	K^c	crystal direction	unit cell direction	equivalent diameter d_s , nm	$D_{ij}^b \times 10^{15}$ m ² /s	$D_{ij}^d \times 10^{15}$ m ² /s
tetragonal	6LYT	1.10	1242	4.4–4.6	0.42	74 ± 2	x	b	0.77	53 ± 0.8	22 ± 2
							y	a	0.84	79 ± 11	82 ± 4
							z	c	1.38	190 ± 7.1	330 ± 20
orthorhombic	1AKI	1.10	1304	8.8–9.2	0.44	13 ± 0.4	x	a	0.74	7.4 ± 0.8	7.1 ± 1.2
							y	c	1.97	304 ± 17	700 ± 45
							z	b	1.01	19 ± 1.1	210 ± 20
triclinic	4LZT	0.24	1269	4.6–4.8	0.33	63 ± 2	x	c	0.79	n.d. ^e	8 ± 0.2
							y	a	0.77	8.6 ± 0.4	6 ± 1.1
							z	b	0.74	12 ± 1.3	5.4 ± 0.8

^a The pH values are both for crystallization and for the CLSM experiments. ^b From Cvetkovic et al.¹⁸; diffusivities for the monoclinic structure could not be calculated due to the low signal-to-noise ratio of our CLSM data. ^c From Cvetkovic et al.²⁴ ^d Calculated using eq 5. ^e n.d. not determined in ref 18.

that cross-diffusivities are dependent on the diagonal diffusivities ($D_{ij} = \sqrt{D_{ii} \cdot D_{jj}}$) and that cross-diffusivities are independent variables, respectively.

Boundary and Initial Conditions. Computations were performed in a rectangular domain large enough to contain the modeled crystal. The initial values (at $t = 0$) of C_p were set to zero in the interior of the crystal (where the binary mask of crystal position has the values 1) and were set to 1 in the subdomain outside the crystal (where the binary mask is zero). As boundary conditions for eq 5, the concentration outside the crystal was kept constant at $C_p = C_{p,0}$ at any time. Considering the sensitivity of the diffusion model on the position of the crystal boundaries, a criterion was added that defines the boundary as the set of points with the highest intensity on a line from the crystal center to the crystal surface. This correction criterion was not automated and it was applied separately for each crystal and rechecked for the datasets at each diffusion time used in the fitting procedure.

Numerical Methods. Equation 5 was discretized with finite differences in the 3-D space on a grid of size ($\Delta x, \Delta y, \Delta z$). A forward explicit discretization in time was found to give sufficient accuracy at time steps between 0.1 and 1 s, and was preferred for simplicity.²⁶ After computing concentration fields at different diffusion times, a Simplex optimization algorithm²⁶ was used to fit the model calculations to the experimental data by varying the diffusion coefficients. A least squares criterion was applied for minimizing the difference between measured profiles of fluorescein in the lysozyme crystals and calculated profiles. The fitting procedure was applied separately for data obtained at three different diffusion times. Diffusivities found in an earlier study¹⁸ were used as input values. The computer program was written by our group in C++ and run on PC desktop computers.

Pore Size Determination. Pore sizes in different crystal directions were determined using the commercial software package PyMOL.²⁷ The positions of the atoms in a specific morphology were imported from the corresponding PDB (Protein Data Bank) file (Table 1) into PyMOL. Complete proteins structures were used, including amino acid side chains, and atoms were represented by their van der Waals radii. Using crystallographic symmetry operations and translations, related molecules were produced and used to build a protein structure of 5–15 nm consisting of unit cells. Three orthoscopic projections of the protein structure were made, one for each orthogonal crystal direction. The projections for tetragonal crystals are presented in Figure 1.

The surface of the pore projection was determined from these images and this surface was used for determination of the pore's surface diameter, d_s (the diameter of the circle with the same surface as a pore cross-section), the parameter characterizing a pore size in this study. Note that the pores consist of rather irregular but repeating segments, leading to relatively wide straight channels and relatively narrow zigzag

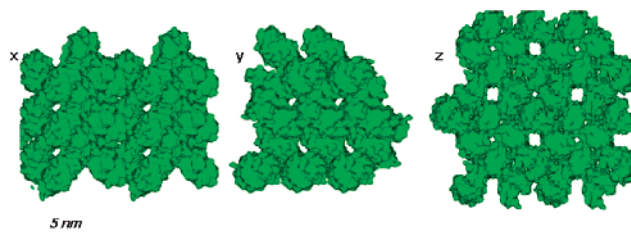


Figure 1. Pore network in three orthogonal directions of tetragonal lysozyme crystals obtained from the 6LYT.pdb file using the commercial software package PyMOL.

channels that intersect with the straight channels.^{1–3} The estimated pore sizes are supposed to be the bottlenecks (smallest diameters) in x , y , and z -direction, respectively.

A Cartesian coordinate system and its origin have been defined for each protein crystal used.¹⁸ The x -coordinate is parallel to the short side of the crystal in the CLSM image while the y -coordinate is perpendicular to x along the long side. Consequently, the z -coordinate represents the direction describing the crystal thickness perpendicular to the CLSM image. The same approach was used for all crystal structures. Using crystallographic knowledge the coordinate system used in our study (x, y, z) was connected to the unit cell coordinate system (a, b, c).

Results and Discussion

Determination of the Diffusion Coefficients. For each crystal, the diffusion coefficients were fitted on three datasets obtained at three different diffusion times. The differences between the obtained diffusivities at different times were less than 5%, and their average value is presented as diffusivity in Table 1. These values were independent from the initial estimates of the diffusivities and from the time step used in the procedure (1, 0.5 and 0.1 s). The three sub-models gave comparable values of D_{ij} (data not shown). Because the same diffusion coefficients were found at different times of diffusion, the anisotropic diffusivities presented in Table 1 are concluded to be indeed concentration independent. Therefore, sub-model 1, as the simplest of all proposed models, will be used in further discussions.

A typical example of comparison of experimental data collected by CLSM and calculated fluorescein concentration profiles in the lysozyme crystals is presented in Figure 2 for the tetragonal crystal morphology. The correspondence between the experimental and calculated data is good at the positions shown in Figure 2 and at any other (x, y, z) position in the tetragonal crystals.

(26) Press: W. H.; Flannely, B. P.; Teukolsky, S. A.; Vetterling, W. T. *Numerical Recipes in C: The Art of Scientific Computing*; Cambridge University Press: Cambridge, 1997.

(27) DeLano, W. L. *The PyMOL molecular graphics system*. 2002.

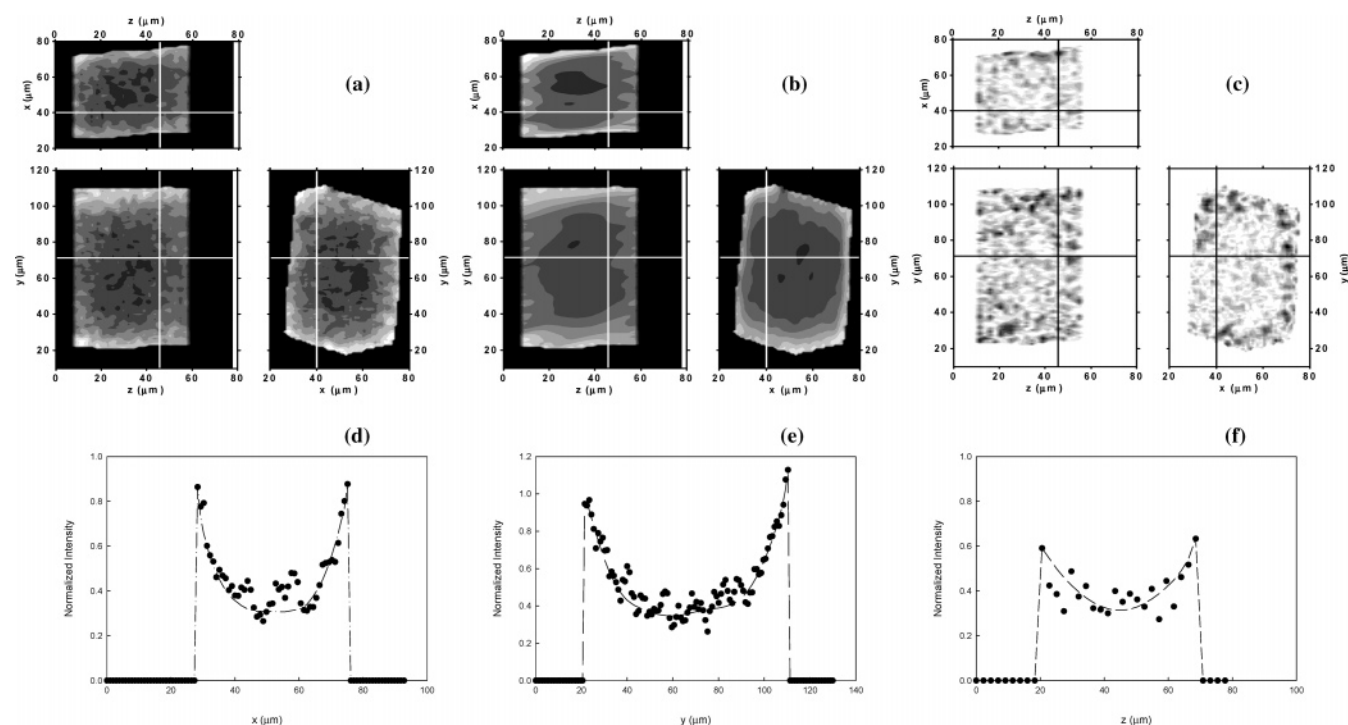


Figure 2. (a) Planar cross-sections of fluorescence intensity data experimentally obtained by CLSM after 744 s of fluorescein diffusion in tetragonal lysozyme crystal; (b) Model-computed solute concentrations at 744 s, shown in a gray scale with darker areas corresponding to lower concentrations; (c) Spatial distribution of the deviation between experimental and computed data (error maps), for the same conditions as (a) and (b). On the gray scale, black areas represent the points with the highest discrepancies and white represent a perfect correspondence; (d–f) Cross-sections of experimental (black points) and calculated (lines) profiles using the 3-D diffusion model. The cross-sections are along planes at $x = 40 \mu\text{m}$, $y = 71.3 \mu\text{m}$, and $z = 45.7 \mu\text{m}$, shown in figures (a–c) as white dotted lines.

Images that represent the difference between the model predictions and experimental data (the error images in Figure 2) showed that deviations were randomly scattered. Therefore, errors were not attributed to the fitting but to the experimental procedure applied. The pixel size was 5 to 20 times bigger than the unit cells of the crystals, providing average information independent of the crystal pore structure. The noise in the CLSM data is in the range of 5–10%, which could explain the level but not the pattern of the noise in Figure 2. The diffusion model assumes that crystals are ideal structures—homogeneous materials with smooth outer surfaces. Crystal defects, crystal surface roughness, charge distribution in the crystals, and heterogeneity of crystals refractive index can cause the observed fluctuations in the experimental concentration profiles. Although these crystal characteristics influence the quality of the acquired images, their influence on the diffusion process is secondary (the model accurately predicts the slopes caused by diffusion in Figure 2) and therefore will not be discussed in detail here. Similar observations were made for other crystals used in the experiments.

Advantages of Presented 3-D Diffusion Models. In our previous study,¹⁸ only initial diffusion profiles were used in a 1-D model, which left some questions about the precision and validity of the determined diffusivities, especially because of the anisotropy. The model based on eq 5 overcomes this problem by using the complete 3-D set of experimental data. The new model gives different values for diffusivities, but predicts similar trends of diffusion anisotropy for the tetragonal morphology.

The model based on eq 5 has obvious advantages over its simplified version¹⁸ due to its higher robustness giving a more realistic representation of the diffusion process and ability to

obtain values for all experimental data (Table 1). The 1-D model is suitable for a quick check on preliminary diffusivities and diffusion anisotropy.

Structural and Diffusion Anisotropy in Protein Crystals—Correlations. Diffusion anisotropy, defined as a disparity in diagonal diffusivities in the crystal, varies per crystal morphology (Table 1). The highest anisotropy was determined for the orthorhombic structure and the lowest for the triclinic structure. The observed anisotropies could not be explained on the basis of the solution characteristics, crystal porosity, crystal density¹⁸ or distribution coefficients²⁴ presented in Table 1. Therefore, we support the hypothesis that diffusion anisotropy is caused by anisotropy of the pore network in the protein crystals, namely in pore size and connectivity.

To test this hypothesis, crystal pore sizes in different crystal directions were determined. A linear correlation was found between the diagonal pore diffusivities and the surface diameter of the pores (Figure 3). This shows that size exclusion is a key mechanism controlling the solute transport in the protein crystals. Considering that protein packing in the crystal determines the size and organization of the pores, the diffusion process will be determined by the protein packing in the crystal structure.

The minimal size of the pore accessible to fluorescein, $d_{s,min}$, was found to be $0.73 \pm 0.06 \text{ nm}$ by using the intercept with the x -axis ($D_{ii} = 0$) of the linear correlation graph $D_{ii}-d_s$ displayed in Figure 3. To be able to correlate $d_{s,min}$ with the size of the solute, the size of the fluorescein molecule is required. Fluorescein is a nonspherical solute with approximate sizes of 0.47, 0.81, and 1.09 nm in different directions. Like the size of a pore, the size of fluorescein was characterized by its surface diameter (d_s). Using the mean projected molecular area of

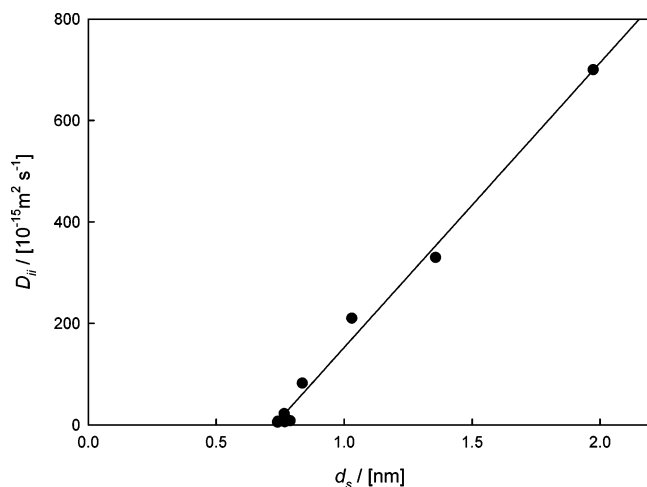


Figure 3. Fluorescein diffusivities, D_{ii} , as a function of pore size, d_s . Markers are experimental data and the line is a linear correlation, $D_{ii} = (-409 \pm 21) + (561 \pm 19) d_s$.

fluorescein, a standard parameter for nonspherical solute size estimation,²³ d_s was found to be 0.69 ± 0.02 nm. The size of fluorescein was within the range of the smallest pore accessible for fluorescein, emphasizing the probability of size exclusion as a key mechanism behind solute diffusion in protein crystals.

Conclusions

The diffusion of fluorescein in lysozyme crystals can be described using an anisotropic model. The levels of anisotropy vary between three different crystal morphologies. The morphology with the highest porosity shows the highest anisotropy

and vice versa. The pore diffusivities and pore sizes correlate linearly. Moreover, the minimum size of the diffusing solute extrapolated from this correlation is almost identical to the size of fluorescein, establishing size exclusion as a key mechanism for solute diffusion in protein crystals. To the authors' knowledge, no such correlation has been established for other mesoporous materials. Thus, the transport of fluorescein in the lysozyme crystals of different morphologies can be approximated by a pore diffusion mechanism for the investigated system. Supplementary understanding would be accomplished if CLSM diffusion experiments were repeated with different sizes of solutes.

Acknowledgment. The Netherlands Organisation for Scientific Research - Chemical Sciences (NWO-CW) funded this work. It has been performed within the International Research Training Group "Diffusion in Porous Materials", jointly supported by NWO (Netherlands) and DFG (Germany). We are thankful to Prof. Dr. S. van der Zwaag and Dr. D. N. Hanlon from The Netherlands Institute for Metals Research, The Netherlands, for providing experimental facilities and support, and Johan Tirell for his contribution in initializing the CLSM measurements. We would like to thank Prof. Dr. Lucas J. van Vliet and Bernd Rieger from TU Delft, The Netherlands, for their help in processing of confocal images. We thank Prof. Dr. A. Freeman from Tel Aviv University, Israel, for help in initial steps of the pore size study and for helpful discussion and critical review of the manuscript.

JA0440708